Available online at www.sciencedirect.com
SCIENCE DIRECT®
Journal of Solid State Chemistry 179 (2006) 103–110
JOURNAL OF SOLID STATE CHEMISTRY
www.elsevier.com/locate/jssc

# Crystal structure and vibrational properies of $Rb_2MgWO_2(PO_4)_2$—A new framework phosphate

M. Mączka[a,*], A. Waśkowska[a], J. Hanuza[a,b]

[a]*Institute of Low Temperature and Structure Research, Polish Academy of Sciences, P.O. Box 1410, 50-950 Wrocław 2, Poland*
[b]*Department of Bioorganic Chemistry, Faculty of Industry and Economics, University of Economics, ul. Komandorska 118/120, 53-345 Wrocław, Poland*

Received 7 July 2005; received in revised form 19 September 2005; accepted 29 September 2005
Available online 15 November 2005

**Abstract**

The new compound $Rb_2MgWO_2(PO_4)_2$ has been synthesized and characterized by a single-crystal X-structure determination, and IR and Raman spectroscopic studies. The crystal structure is orthorhombic, space group *Pbca*, with the unit cell dimensions $a = 9.891(2)$, $b = 12.641(2)$, $c = 15.338(3)$ Å, $Z = 8$. Compared to the $K_2M^{II}WO_2(PO_4)_2$ series, where $M^{II}$ = Mg, Mn, Fe, Co, Ni, and Cd, the volume of the unit cell in the present compound is nearly doubled. The $MgO_6$ and $WO_6$ octahedra are arranged into polyhedral groups consisting of two edge sharing $MgO_6$ joined by corners with two $WO_6$ octahedra. These groups are interconnected through the $PO_4$ tetrahedra into layers in $a \times b$ plane. The $Rb^+$ ions perform thermally activated displacements within the cavities formed between the polyhedral layers. The origin of various Raman and IR modes is discussed. These results indicate that a clear energy gap exists between the stretching and remaining modes. The most intense modes are shown to be due to vibrations of the W–O bonds.
© 2005 Elsevier Inc. All rights reserved.

*Keywords:* $Rb_2MgWO_2(PO_4)_2$; Phosphate; Crystal structure; Phonon properties

## 1. Introduction

Titanyl orthophosphates, $ATiOPO_4$ ($A$ = Na, K, Rb, Cs, Tl, Ag) are well known nonlinear optical (NLO) materials of technological importance [1–5]. These compounds exhibit a high-temperature phase transition from *Pnan* to *Pna2₁* space group [6,7]. It has been shown that the same type of structure can be obtained by replacing $Ti^{IV}$ ions by $M$ = Zr, Sn, Nb, Ta or Sb, and/or $P^V$ atoms by $B$ = As, Si or Ge atoms [8–11]. The general formula of these compounds can therefore be written as $AMOBO_4$. It is also possible to replace two $Ti^{IV}$ ions by two cations of different valencies. So far this kind of replacement has been accomplished for potassium analogues of $KTiOPO_4$ (KTP) with $Ti^{IV}$ ions replaced by $Mg^{II}$ and $Nb^V$ ions, or by $W^{VI}$ and $M^{II}$ = Mg, Ni, Co, Fe, Mn, Cd ions [12–15]. The chemical formulas of these compounds are: $K(Mg_{1/3}Nb_{2/3})PO_5$ [12] and $K_2MWO_2(PO_4)_2$ [13–15]. In contrary to the $AMOBO_4$ phosphates, $K(Mg_{1/3}Nb_{2/3})PO_5$ and $K_2MWO_2(PO_4)_2$ are not isostructural with KTP, although their crystal structures are closely related to KTP. $K(Mg_{1/3}Nb_{2/3})PO_5$ crystallizes in the *P4₁22* space group, and shows a disordered structure with statistical distribution of Nb and Mg at the same sites [12]. Besides, this compound does not exhibit any phase transition. $K_2MWO_2(PO_4)_2$ phosphates crystallize in the *P4₁2₁2* space group and exhibit an ordered structure. Except for $K_2NiWO_2(PO_4)_2$ [13], the compounds form a class of materials exhibiting different phase transitions of structural and ferroic nature in the temperature range of 100–870 K [14,15]. In particular, $K_2MgWO_2(PO_4)_2$ was shown to exhibit at least three ferroelastic and ferroelectric phase transitions above room temperature [15]. A common feature of the crystal structures of the $K_2MWO_2(PO_4)_2$ compounds is the oxygen framework built of corner sharing $M^{II}O_6$ and $WO_6$ octahedral chains interconnected via $PO_4$ tetrahedra into the three-dimensional network with the cavities of different geometry. The dynamics of the $K^+$ ions located in the cavities contribute to the temperature-dependent phase transitions and anomalous behaviour of electrical conductivity [14,15]; however, the question which structural units are the major contributors to the NLO properties is still under discussion.

*Corresponding author. Fax: +48 71 344 1029.
*E-mail address:* m.maczka@int.pan.wroc.pl (M. Mączka).

0022-4596/$ - see front matter © 2005 Elsevier Inc. All rights reserved.
doi:10.1016/j.jssc.2005.09.049

Synthesis of di-rubidium magnesium tungsten dioxide *bis*(phosphate), abbreviated $Rb_2MgWP$, was undertaken in search for new NLO materials, being the close analogues of KTP, in which $K^+$ ions have been replaced by $Rb^+$ ions, and two symmetrically nonrelated $Ti^{IV}$ ions have been replaced by $Mg^{II}$ and $W^{VI}$. In the present paper we report single-crystal X-ray diffraction, Raman and IR studies of $Rb_2MgWO_2(PO_4)_2$ phosphate in order to describe the principal structure characteristics. Our results show that whereas replacement of $K^+$ by $Rb^+$ ions in KTP does not change the crystal structure, the replacement of $K^+$ by $Rb^+$ in $K_2MgWO_2(PO_4)_2$ leads to the essential modification in the crystal structure. As a result, $Rb_2MgWO_2(PO_4)_2$ crystallizes in a new type of orthorhombic structure, not isostructural with KTP or $K_2MgWO_2(PO_4)_2$ and even not related to these structures.

## 2. Experiment

Single crystals of $Rb_2MgWP$ were grown by cooling of the molten, stoichiometric mixture of MgO, $Rb_2CO_3$, $WO_3$ and $P_2O_5$. The mixture was kept at 800 °C for 20 h, cooled with a 1 °C/h rate to 700 °C and 5 °C/h rate down to room temperature. The obtained colourless crystals of optical quality were separated from the solidified flux with hot water. The crystal composition was checked with the help of X-ray dispersion measurements using a Philips SEM 515 scanning electron microscope and EDAX 9800 microanalyzer. This method showed that the Rb:Mg:W:P ratio is approximately 31.6:16.1:15.9:36.4, what agrees with the $Rb_2MgWO_2(PO_4)_2$ composition within experimental error of this method.

Polycrystalline infrared spectra were measured with a Biorad 575C FT–IR spectrometer as KBr pellets in the 1500–400 $cm^{-1}$ region and in Nujol suspension for the 500–30 $cm^{-1}$ region. Raman spectra were recorded in 180° scattering geometry with a Bruker FT-Raman RFS 100/S spectrometer. Excitation was performed with a 1064 nm line of a YAG:$Nd^{3+}$ laser. Blackman–Harris four-term apodization was applied and the number of collected scans was 64. The IR and Raman spectra were recorded with a spectral resolution of 2 $cm^{-1}$.

A sample of dimensions given in Table 1 was chosen for X-ray diffraction measurements on a single-crystal Oxford Diffraction/CCD X-calibur diffractometer, operating in $\kappa$ geometry and using graphite monochromated Mo$K\alpha$ radiation. The intensity data were collected with $\omega$-scan technique and steps of $\Delta\omega = 1.2°$. The exposure time was 20 s/image. The 1225 K images taken in eight sets of 153 exposures at different $\omega$ positions covered about 98% of the Ewald sphere. Crystal and instrument stability was controlled by one image, selected as a standard and measured after each 60 images [16]. The intensities, corrected for Lorentz-polarization effects, were integrated and numerical absorption correction based on the crystal shape was applied [17]. The structure was solved with Patterson method using the SHELXS97 program [18] and subsequent difference Fourier calculations. The structure refinement calculations were performed with the SHELXL99 package [19]. Crystal data and further experimental details are summarized in Table 1 together with the parameters of the structure refinements.

Table 1
Crystal data, experimental details and structure refinement results for $Rb_2MgWO_2(PO_4)_2$

| | |
|---|---|
| *Crystal data* | |
| Temperature (K) | 297 |
| Crystal system, space group | Orthorhombic, *Pbca* |
| Unit cell dimensions (Å) | |
| *a* | 9.891(2) |
| *b* | 12.641(2) |
| *c* | 15.338(3) |
| Volume (Å$^3$) | 1917.7(3) |
| *Z*, calculated density (Mg/m$^3$) | 8,4.163 |
| Crystal size (mm) | 0.21 × 0.18 × 0.17 |
| *Data collection* | |
| Wavelength (Å) | 0.71073 |
| 2$\theta$ max for data collection | 65.15 |
| Limiting indices: | |
| *h* | −14, 13 |
| *k* | −15, 18 |
| *l* | −23, 20 |
| Reflections collected | 28462 |
| Reflections unique | 3454 |
| Reflections [$>2\sigma(I)$] | 2356 |
| Absorption coefficient (mm$^{-1}$) | 22.57 |
| Absorption correction | Numerical |
| *R*(int) before, after abs. correction | 0.138, 0.062 |
| $T_{min}$, $T_{max}$ | 0.127, 0.322 |
| *Refinement* | |
| Refinement method | Full-matrix least-squares on $F^2$ |
| Number of refined parameters | 146 |
| Goodness-of-fit on $F^2$ | 0.996 |
| Final *R* indices [$I>2\sigma(I)$] | |
| $R_1$ | 0.0264 |
| w$R_2$ | 0.0338 |
| Extinction coefficient | 0.00211(2) |
| Largest diff. peak and hole (eÅ$^{-3}$) | 1.69 and −1.67 |

## 3. Results and discussion

### 3.1. Single-crystal X-ray diffraction studies

The structure of $Rb_2MgWP$ adopts centrosymmetric space group *Pbca* with lattice parameters given in Table 1. The unit cell volume is doubled compared to those of the $K_2M^{II}WO_2(PO_4)_2$ crystal series, which all retain the volume of the parent KTP phosphate. All atoms occupy general positions and their final parameters together with the equivalent thermal displacement parameters $U_{eq}$ are listed in Table 2. Tables 3 and 4 give selected bond lengths and anisotropic displacement parameters, respectively. Supplementary data are available from the Fachinformationszentrum (FIZ) Karlsruhe, Informationsdienste ICSD,

Table 2
Atomic coordinates ($\times 10^4$) and equivalent isotropic displacement parameters ($Å^2 \times 10^3$) for $Rb_2MgWO_2(PO_4)_2$

| | x | y | Z | U(eq) |
|---|---|---|---|---|
| W(l) | 7483(1) | 5072(1) | 3580(1) | 5(1) |
| Rb(l) | 8895(1) | 6737(1) | 1570(1) | 27(1) |
| Rb(2) | 3906(1) | 3661(1) | 3862(1) | 38(1) |
| Mg(l) | 9998(1) | 6309(1) | 5027(1) | 7(1) |
| P(l) | 7579(1) | 7560(1) | 4055(1) | 6(1) |
| P(2) | 10,753(1) | 5050(1) | 3342(1) | 6(1) |
| O(1) | 6231(3) | 7571(2) | 4495(2) | 12(1) |
| O(2) | 8748(3) | 7502(2) | 4676(2) | 13(1) |
| O(3) | 7676(3) | 6614(2) | 3401(2) | 11(1) |
| O(4) | 7722(3) | 8530(2) | 3427(2) | 13(1) |
| O(5) | 10,889(3) | 6064(2) | 3875(2) | 10(1) |
| O(6) | 10,975(3) | 4037(2) | 3872(2) | 12(1) |
| O(7) | 11,921(2) | 5092(2) | 2652(2) | 11(1) |
| O(8) | 9386(2) | 5007(2) | 2844(2) | 9(1) |
| O(9) | 8542(2) | 4998(2) | 4501(2) | 12(1) |
| O(10) | 5924(3) | 5215(2) | 4070(2) | 15(1) |

U(eq) is defined as one-third of the trace of the orthogonalized $U_{ij}$ tensor.

D-76344 Eggenstein-Leopoldshafen, Germany (e-mail: crysdata@fiz-karlsruhe.de) under the CSD number 415569 (filename RbMgWPO.cif).

The crystal host lattice consists of two edge sharing $MgO_6$ octahedra connected by corners with two $WO_6$ octahedra. These groups are linked by $PO_4$ tetrahedra into the characteristic three-dimensional framework (Fig. 1). Two symmetrically independent Rb-atoms are located in the large cavities. Rb(1) is coordinated by eight O-atoms in the distances ranging from 2.948(3) to 3.168(3) Å, while Rb(2) is surrounded by 7 + 2 oxygen atoms at the distances from 2.818(3) to 3.481(3) Å (Table 3). Relatively high values of anisotropic thermal displacement amplitudes of $Rb^+$ indicate that these loosely bound ions perform thermally activated movements within the framework cages (Table 4). Two distinct phosphate groups do not retain a regular symmetry as typically in KTP [9] and $TlTiOPO_4$ [6]. The P(1)$O_4$ tetrahedron is quite distorted (Table 3), as one of its edges between O(3) and O(4), links the W-centered octahedra into the chain running parallel to the *b*-axis (Fig. 1). The O(1) and O(2) corners of the same tetrahedron join the $MgO_6$ octahedra building in this way the polyhedral layer in the $a \times b$ plane. The P(2)$O_4$ tetrahedron is more regular (Table 3). Two shorter P(2)–O bonds maintain the sequence –P(2)–O(5)–Mg–O(6)–P(2′)–, while the atoms O(7) and O(8) link two symmetry-related $WO_6$ octahedra (Fig. 2).

The $MgO_6$ and $WO_6$ octahedra are also distorted but the latter show much wider spread of bond distances. In $MgO_6$ there are four shorter bonds ranging from 1.992(3) to 2.023(3) Å, corresponding to Mg–O–P(2) and Mg–O–P(1) connections, respectively. Two longer bonds with O(9) and O(9′) [2.311(3) and 2.339(3) Å, respectively], are involved in bridging the $MgO_6$ and $WO_6$ octahedra (Fig. 2). In the group formed by two $MgO_6$ and two $WO_6$ octahedra the

Table 3
Selected bond lengths (Å) for $Rb_2MgWO_2(PO_4)_2$

| | |
|---|---|
| W(1)–O(10) | 1.725(3) |
| W(1)–O(9) | 1.761(3) |
| W(1)–O(7)#1 | 1.969(3) |
| W(1)–O(4)#2 | 1.974(2) |
| W(1)–O(3) | 1.978(2) |
| W(1)–O(8) | 2.196(2) |
| Mg(1)–O(6)#3 | 1.992(3) |
| Mg(1)–O(5) | 1.999(3) |
| Mg(1)–O(1)#4 | 2.007(3) |
| Mg(1)–O(2) | 2.023(3) |
| Mg(1)–O(9)#3 | 2.311(3) |
| Mg(1)–O(9) | 2.339(3) |
| P(1)–O(1) | 1.495(3) |
| P(1)–O(2) | 1.499(3) |
| P(1)–O(3) | 1.564(2) |
| P(1)–O(4) | 1.565(3) |
| P(2)–O(5) | 1.527(3) |
| P(2)–O(6) | 1.532(3) |
| P(2)–O(8) | 1.553(3) |
| P(2)–O(7) | 1.568(3) |
| Rb(1)–O(10)#5 | 2.948(3) |
| Rb(1)–O(8) | 2.973(3) |
| Rb(1)–O(6)#6 | 2.989(3) |
| Rb(1)–O(1)#5 | 3.020(3) |
| Rb(1)–O(3) | 3.059(3) |
| Rb(1)–O(2)#7 | 3.065(3) |
| Rb(1)–O(7)#1 | 3.092(3) |
| Rb(1)–O(5)#1 | 3.168(3) |
| Rb(2)–O(10) | 2.818(3) |
| Rb(2)–O(6)#8 | 2.938(3) |
| Rb(2)–O(1)#9 | 2.965(3) |
| Rb(2)–O(2)#2 | 3.015(3) |
| Rb(2)–O(8)#1 | 3.157(3) |
| Rb(2)–O(7)#8 | 3.252(3) |
| Rb(2)–O(5)#2 | 3.289(3) |
| Rb(2)–O(4)#2 | 3.405(3) |
| Rb(2)–O(10)#9 | 3.481(3) |
| W(1)–Rb(1) | 3.9854(7) |
| W(1)–Rb(2) | 3.9860(8) |
| W(1)–Rb(1)#1 | 4.1318(8) |

Symmetry transformations used to generate equivalent atoms: #1: $x-\frac{1}{2}, y, -z+\frac{1}{2}$; #2: $-x+\frac{3}{2}, y-\frac{1}{2}, z$; #3: $-x+2, -y+1, -z+1$; #4: $x+\frac{1}{2}, -y+\frac{3}{2}, -z+1$; #5: $x+\frac{1}{2}, y, -z+\frac{1}{2}$; #6: $-x+2, y+\frac{1}{2}, -z+\frac{1}{2}$; #7: $x, -y+\frac{3}{2}, z-\frac{1}{2}$; #8: $x-1, y, z$; #9: $-x+1, -y+1, -z+1$.

W–O(9) distance is much shorter than the Mg–O(9) and Mg–O(9′) separations [1.765(3), compared to 2.307(4) and 2.335(4) Å, respectively]. It is also worth noting that one of the W–O bonds in the $WO_6$ octahedron [W–O(10), 1.725(3) Å] is terminal. This configuration is different from that observed for KTP analogues, containing $TiO_6$, $ZrO_6$, $SnO_6$, $SbO_6$, $NbO_6$ or $TaO_6$ octahedra. The difference may be attributed to the strength of $M$–O$\cdots M'$ bridges connecting the octahedra into infinite chains in the structure of KTP type (O$\cdots M'$ denotes the longer metal–oxygen distance in the bridge). In case of tetravalent or pentavalent atoms, like Ti, Zr, Sb, etc., the O$\cdots M'$ bonds are relatively strong and the octahedral chains are

Table 4
Anisotropic displacement parameters ($Å^2 \times 10^3$) for $RbMgWO_2(PO_4)_2$

| | $U_{11}$ | $U_{22}$ | $U_{33}$ | $U_{23}$ | $U_{13}$ | $U_{12}$ |
|---|---|---|---|---|---|---|
| W(1) | 6(1) | 4(1) | 4(1) | 0(1) | 0(1) | 0(1) |
| Rb(1) | 26(1) | 21(1) | 33(1) | 13(1) | 9(1) | 4(1) |
| Rb(2) | 17(1) | 33(1) | 63(1) | 27(1) | −7(1) | −5(1) |
| Mg(1) | 10(1) | 7(1) | 6(1) | 0(1) | 1(1) | 0(1) |
| P(1) | 8(1) | 4(1) | 7(1) | 0(1) | 0(1) | 0(1) |
| P(2) | 7(1) | 7(1) | 5(1) | 1(1) | 1(1) | 0(1) |
| O(2) | 15(2) | 6(1) | 18(2) | −3(1) | −5(1) | 2(1) |
| O(1) | 10(1) | 6(1) | 21(2) | 2(1) | 2(1) | 2(1) |
| O(3) | 19(2) | 3(1) | 10(1) | −2(1) | 2(1) | 2(1) |
| O(4) | 22(2) | 9(1) | 8(1) | 1(1) | 4(1) | 1(1) |
| O(5) | 15(2) | 9(1) | 7(1) | −5(1) | 2(1) | −1(1) |
| O(6) | 13(1) | 11(1) | 11(2) | 5(1) | 2(1) | −1(1) |
| O(7) | 9(1) | 15(1) | 7(1) | 0(1) | 2(1) | −1(1) |
| O(8) | 8(1) | 11(1) | 8(1) | 1(1) | −1(1) | 0(1) |
| O(9) | 8(1) | 16(1) | 11(1) | −2(1) | 2(1) | −2(1) |
| O(10) | 13(1) | 13(1) | 19(2) | 0(1) | 5(1) | −1(1) |

The anisotropic displacement factor exponent takes the form: $-2\pi^2(h^2a^{*2}U_{11}+\cdots+2hka^*b^*U_{12})$.

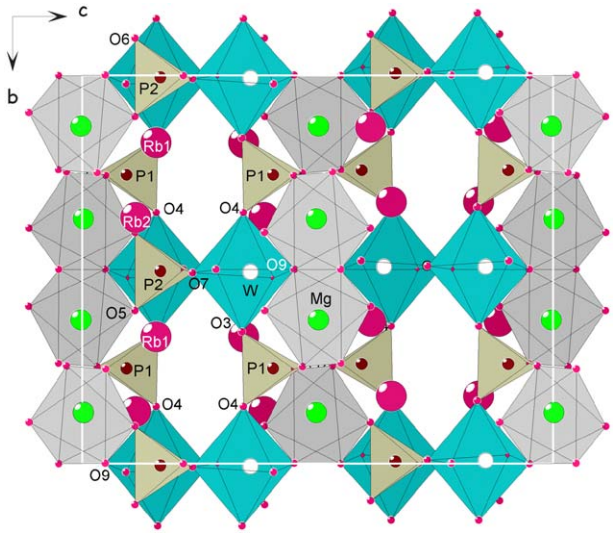


Fig. 1. Crystal structure of $Rb_2MgWO_2(PO_4)_2$ showing the presence of tunnels.

not broken when small $K^+$ cations are replaced with much larger $Rb^+$ or $Cs^+$ ions. In the $M^I_2MgWO_2(PO_4)_2$ structure, however, the O···Mg interaction within the W–O···Mg bridge is relatively weak. Therefore, whereas the $K_2MgWO_2(PO_4)_2$ structure is related to the structure of KTP, the substitution of larger $Rb^+$ for smaller $K^+$ leads to the new type of structure with broken chains.

### 3.2. Selection rules and vibrational modes

The factor group analysis predicts that there should be $48A_g+48B_{1g}+48B_{2g}+48B_{3g}+48A_u+47B_{1u}+47B_{2u}+47B_{3u}$ ($\boldsymbol{k}=0$) optic and $B_{1u}+B_{2u}+B_{3u}$ acoustic unit cell modes for the orthorhombic *Pbca* structure. Since P–O and W–O bonds are much stronger than the Mg–O or Rb–O

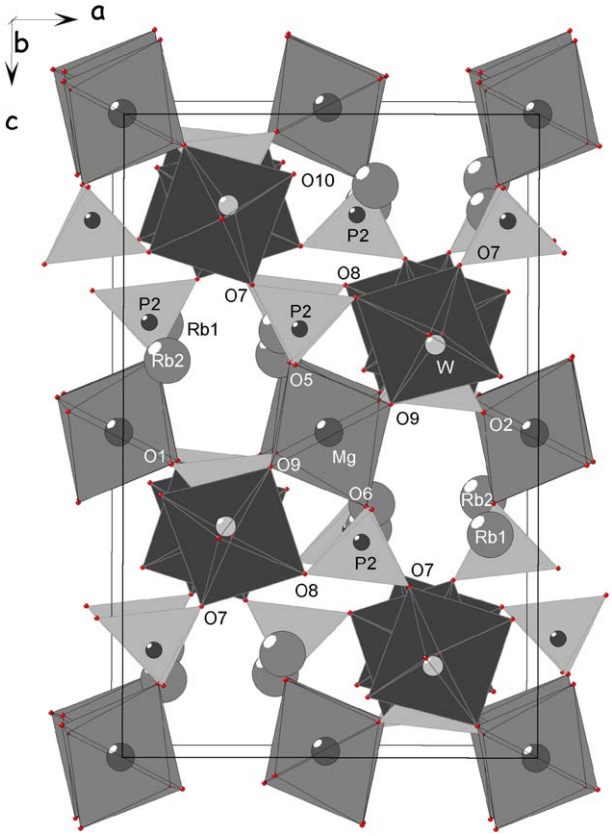


Fig. 2. Projection of the $Rb_2MgWO_2(PO_4)_2$ crystal structure along the *b*-axis.

bonds, from the spectroscopic point of view the structure can be considered as built of $PO_4^{3-}$ and $WO_6$ molecular groups and $Rb^+$ and $Mg^{2+}$ cations. The vibrational modes can, therefore, be subdivided into $6A_g+6B_{1g}+6B_{2g}+6B_{3g}+6A_u+6B_{1u}+6B_{2u}+6B_{3u}$ translational motions of $Rb^+$ ions, $3A_g+3B_{1g}+3B_{2g}+3B_{3g}+3A_u+3B_{1u}+3B_{2u}+3B_{3u}$ translational motions of $Mg^{2+}$ ions, $3A_g+3B_{1g}+3B_{2g}+3B_{3g}+3A_u+3B_{1u}+3B_{2u}+3B_{3u}$ translational motions of $WO_6$ polyhedra, $6A_g+6B_{1g}+6B_{2g}+6B_{3g}+6A_u+6B_{1u}+6B_{2u}+6B_{3u}$ translational motions of $PO_4^{3-}$ ions, and $30A_g+30B_{1g}+30B_{2g}+30B_{3g}+30A_u+30B_{1u}+30B_{2u}+30B_{3u}$ modes describing internal and librational motions of the $WO_6$ polyhedra and $PO_4^{3-}$ ions. It should be noticed, however, that from the $18A_g+18B_{1g}+18B_{2g}+18B_{3g}+18A_u+18B_{1u}+18B_{2u}+18B_{3u}$ translational modes, the $B_{1u}+B_{2u}+B_{3u}$ acoustic modes should be subtracted. The "g" modes are Raman active, $B_{1u}$, $B_{2u}$ and $B_{3u}$ are IR active and $A_u$ modes are inactive.

The IR and Raman spectra are presented in Figs. 3–5, and the measured wavenumbers are listed in Table 5. It can be seen that the spectra consist of two separated regions: 1200–830 and 660–50 $cm^{-1}$. The bands observed in the first region can be assigned to the stretching modes and those below 660 $cm^{-1}$ to the bending and lattice modes. Such a clear separation of two regions was not observed in the case of KTP and RTP crystals. This difference can be related to the shift of the $WO_6$ stretching modes towards

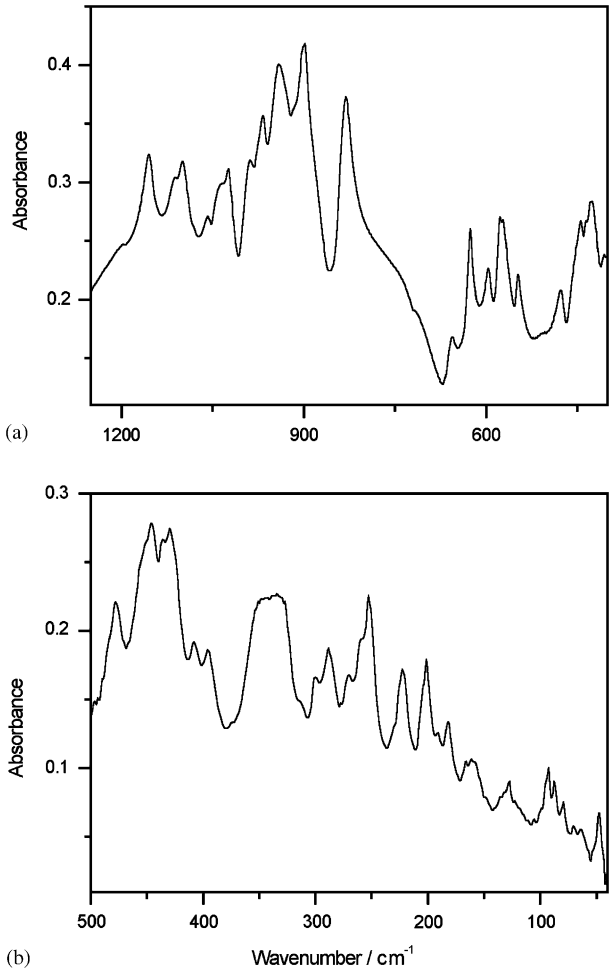


Fig. 3. Polycrystalline infrared spectrum of $Rb_2MgWO_2(PO_4)_2$ in the mid-IR (a) and far-IR (b) regions.

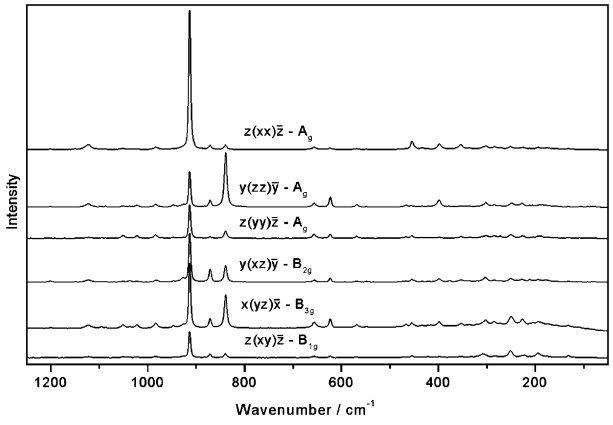


Fig. 4. Polarized Raman spectra of $Rb_2MgWO_2(PO_4)_2$.

higher frequencies when compared to the $TiO_6$ stretching modes due to weak interaction of the $WO_6$ octahedra with $Mg^{2+}$ ions and higher valence of the tungsten atoms with respect to titanium atoms.

The stretching modes can be subdivided into stretching vibrations of the $PO_4^{3-}$ ions and $WO_6$ groups. The $PO_4^{3-}$ free ion, having $T_d$ symmetry, should exhibit the presence

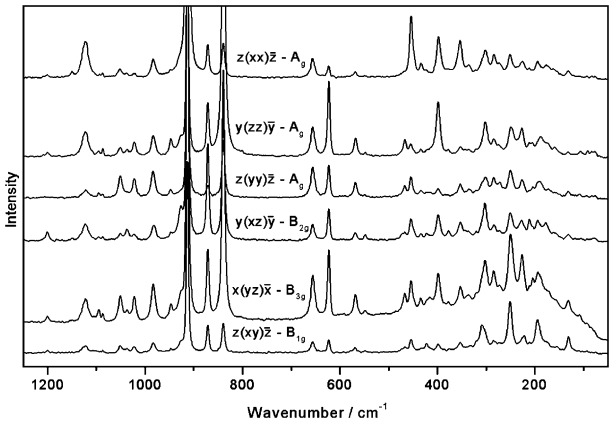


Fig. 5. Enlarged polarized Raman spectra of $Rb_2MgWO_2(PO_4)_2$ showing details for weak modes.

of $\nu_1(A_1) = 938\,cm^{-1}$ and $\nu_3(F_2) = 1017\,cm^{-1}$ stretching modes [20]. The $A_1$ mode is Raman active and $F_2$ mode is both IR and Raman active. In the $Rb_2MgWP$ phosphate these modes should be observed both in IR- and Raman spectra and $F_2$ mode should split into triplet for every polarization configuration. Because there are two crystallographically nonequivalent phosphate ions, for every polarization configuration the $2\nu_1(PO_4)$ and $6\nu_3(PO_4)$ components should be present. As far as the $WO_6$ octahedron with $O_h$ symmetry is concerned, three stretching modes: $\nu_1(A_{1g})$, $\nu_2(E_g)$ and $\nu_3(F_{1u})$ [20] have to be expected. The $\nu_1$ and $\nu_2$ modes are Raman-active and the $\nu_3$ mode is IR-active. The $\nu_2$ and $\nu_3$ modes should split into two and three components, respectively.

The former studies of a number of titanyl and niobyl phosphates showed that the $\nu_1$ and $\nu_3$ modes of the $PO_4^{3-}$ ions are observed around 933–1000 and 970–1150 $cm^{-1}$, respectively [21–25]. The stretching modes of $TiO_6$ and $NbO_6$ octahedra were located in the 600–850 and 630–890 $cm^{-1}$ region, respectively [21–25]. It has been shown that the strongest Raman line can be attributed to the $\nu_1$ symmetric stretching mode of the $TiO_6$ ($NbO_6$) unit. This band shifts towards higher frequency with increasing ion valency (from 650–710 $cm^{-1}$ for $TiO_6$ to around 870–890 $cm^{-1}$ for $NbO_6$ [21–25]). In the present crystal a very strong Raman band at 913 $cm^{-1}$ can unambiguously be assigned to the $\nu_1(WO_6)$ mode. This band is strongly polarized and it shows most of its intensity when both the incident and scattered light is polarized along direction parallel to the tunnels occupied by $Rb^+$ ions, i.e. for the $xx$ polarization. This effect is very similar to the behaviour of KTP. It is remarkable that scattering intensity of this mode for the $xx$ polarization is very large and its bandwidth is very small (only 4.6 $cm^{-1}$). Since in the stimulated Raman effect the amplification of a Raman line is proportional to the spontaneous Raman scattering cross-section and inversely proportional to the linewidth of the corresponding Raman line, this mode can probably contribute to efficient stimulated Raman scattering. We may also observe two Raman modes at 871 and 839 $cm^{-1}$. Since

Table 5
Raman and IR wavenumbers for $Rb_2MgWO_2(PO_4)_2$

| Raman | | | | | | IR | Assignment |
|---|---|---|---|---|---|---|---|
| $y(zz)\bar{y}$ $A_g$ | $z(xx)\bar{z}$ $A_g$ | $z(yy)\bar{z}$ $A_g$ | $y(xz)\bar{y}$ $B_{2g}$ | $x(yz)\bar{x}$ $B_{3g}$ | $z(xy)\bar{z}$ $B_{1g}$ | | |
| 1200w | — | — | 1201w | 1200w | — | 1196w | $\nu_3(PO_4)$ |
| — | 1148vw | — | — | — | — | 1155s | |
| 1123m | 1123m | 1121w | 1122m | 1122m | 1122w | 1111m | |
| 1095w | — | 1095vw | 1095vw | 1095w | — | 1098m | |
| 1087w | 1087vw | 1087vw | 1087vw | 1086w | 1086vw | 1071w | |
| 1050w | 1051w | 1050m | 1050w | 1050m | 1050w | 1035m | |
| 1036w | 1038vw | — | 1037w | 1036w | 1036w | 1023m | |
| 1021w | 1021w | 1021m | 1022w | 1021m | 1021w | 988w | |
| 983w | 983w | 984m | 982m | 984m | 984w | 967m | |
| 947w | — | 947w | 947w | 946w | 946vw | 940s | $\nu_1(PO_4)$ |
| 925w | — | — | 926w | 924w | 924w | 902s | |
| — | — | — | — | — | — | 898s | |
| 913s | 913vs | 913s | 913s | 913s | 913s | 914w | $\nu_1(WO_6)$ |
| 871m | 871m | 871m | 871m | 871m | 871m | — | $\nu_2(WO_6)$ |
| 839s | 839m | 839m | 839s | 839s | 839m | 830s | $\nu_3(WO_6)$ |
| 656m | 656w | 656m | 656w | 655m | 655w | 655w | $\nu_4(PO_4)$ |
| 623m | 623w | 623m | 623m | 623m | 623w | 626m | |
| — | — | — | — | — | — | 597w | |
| 567w | 568w | 568w | 568w | 568w | 568w | 577m | |
| — | — | — | — | — | — | 572m | |
| — | — | — | 547w | 548w | 548vw | 547w | |
| — | — | — | 471w | — | — | 477w | $\nu_2(PO_4)$ |
| 466w | — | 466w | 466w | 466w | 466vw | — | |
| 455w | 454m | 454w | 454m | 454m | 454w | 445w | |
| 433vw | 433w | 433vw | 433w | 434w | 432vw | 436vw | $\nu_4(WO_6)$ |
| 420vw | 422vw | 423vw | 422w | 421vw | 422w | 430m | |
| — | — | 415vw | — | 415vw | — | 408w | |
| 399m | 398m | 399w | 399m | 399m | 399w | 396w | $\nu_5(WO_6)$ |
| 377vw | 379vw | 377vw | 376w | 377vw | — | — | $T'$(Mg) |
| 352w | 353m | 352w | 352m | 352w | 353w | 346s | |
| 335vw | 335w | 335vw | 335vw | 335w | 330vw | 334s | |
| 320vw | — | 320vw | 320vw | 320vw | — | 314vw | $T'(PO_4)$ and $L(PO_4)$ |
| — | — | — | 308sh | 308sh | 308m | — | |
| 301m | 301m | 301w | 302m | 302m | — | 300w | |
| 284w | 284w | 285w | 284w | 285w | 285w | 288m | |
| 274w | 273vw | 272w | 272vw | 272vw | — | 270w | |
| — | — | — | — | — | — | 258sh | |
| 249m | 251m | 250m | 251m | 250m | 251m | 253m | $\nu_6(WO_6)$ |
| 226m | 225w | 226w | 227w | 226m | 221w | 223m | $T'(PO_4)$ and $L(PO_4)$ |
| 211w | 212vw | — | 211w | 210vw | — | — | |
| 205w | — | 204vw | — | 204w | — | 202m | |
| 187w | 193w | 189w | 193w | 193m | 194m | 191vw | |
| 174sh | 176w | 172vw | 177w | 171w | 176sh | 182w | |
| 159w | 162vw | — | 161vw | — | — | 166vw | |
| — | — | — | 156vw | 156vw | 155w | 160w | |
| 132w | 130w | 132w | 130w | 132w | 131w | 127w | $T'$(W), $L(WO_6)$ and |
| 105w | 109vw | 107vw | — | 107vw | — | — | $T'$(Rb) |
| 91w | 92vw | 93vw | — | 93vw | — | 93w | |
| 85w | 82vw | 82vw | — | — | — | 88w | |
| | | | | | | 79w | |
| | | | | | | 71vw | |
| | | | | | | 63vw | |
| | | | | | | 47w | |

vs. s, sh, m, w and vw denote very strong, strong, shoulder, medium, weak and very weak, respectively

the former band does not have any counterpart in the IR spectrum, we assign this band to the $\nu_2$ asymmetric stretching mode of the $WO_6$ group. The remaining band at 839 $cm^{-1}$ can be most likely assigned to the $\nu_3(WO_6)$. The $\nu_1$ and $\nu_3$ modes of the $PO_4^{3-}$ ion are observed at 898–947 and 967–1201 $cm^{-1}$, respectively. The frequency of the $\nu_3(PO_4)$ modes is higher than that observed for the titanyl (990–1130 $cm^{-1}$) [21–23] and niobyl phosphates (1000–1140 $cm^{-1}$) [24,25]. Since the study of Na SuperIonic Conductor (NASICON)-type phosphates revealed frequency increase with increasing covalent character of the metal–oxygen bonds within *M*–O–P bridge [26], the observed frequency increase in $Rb_2MgWP$ can be explained as a result of stronger covalent character of the W–O bonds when compared with the Nb–O and Ti–O bonds. The splitting of the $\nu_3(PO_4)$ mode is also larger (234 $cm^{-1}$) than that observed for the titanyl phosphates ($\sim$140 $cm^{-1}$) due to large distortion of the $PO_4^{3-}$ tetrahedra.

In the bending modes region one should observe symmetric and asymmetric bending modes of the $PO_4^{3-}$ ions ($\nu_2(PO_4)$ and $\nu_4(PO_4)$, respectively). These modes are seen at 420 and 567 $cm^{-1}$ for a free phosphate ion [20]. The remaining bending modes can be attributed to the $WO_6$ group. For a free $WO_6$ octahedron with the $O_h$ symmetry three bending modes should be observed: $\nu_4(F_{1u})$, $\nu_5(F_{2g})$ and $\nu_6(F_{2u})$. The former studies of a number of phosphates showed that the $\nu_4(PO_4)$ modes are usually well separated from the $\nu_2(PO_4)$ modes, giving rise to bands in the 490–670 $cm^{-1}$ region [24–27]. In case of $Rb_2MgWP$ we may unambiguously assign the group of bands in the 540–660 $cm^{-1}$ region to the $\nu_4(PO_4)$ modes. The $\nu_2(PO_4)$ modes were observed for the titanyl and niobyl phosphates at 370–430 $cm^{-1}$ [21–25]. Since, however, the $\nu_4(PO_4)$ modes are observed at significantly higher frequency than in the titanyl and niobyl phosphates, the same behaviour may be expected for the $\nu_2(PO_4)$ modes. Moreover, the study of $Na_2Cr_2(PO_4)_3$ has shown that for this compound, having very similar frequency range of the $\nu_4(PO_4)$ modes (545–670 $cm^{-1}$ [26]), the $\nu_2(PO_4)$ modes are present at 450–470 $cm^{-1}$. We assign, therefore, the 450–480 $cm^{-1}$ bands to the $\nu_2(PO_4)$ modes. The $\nu_4(TiO_6)$, $\nu_5(TiO_6)$ and $\nu_6(TiO_6)$ bending modes were located for KTP either at 323, 269 and 213 $cm^{-1}$ [21] or at 460–500, 320–385 and 220–290 $cm^{-1}$ [23]. In case of niobyl phosphates, the bands observed near 450, 350 and 270 $cm^{-1}$ were assigned to $\nu_4(NbO_6)$, $\nu_5(NbO_6)$ and $\nu_6(NbO_6)$ modes, respectively [24,25]. Since $\nu_5$ mode of an octahedron gives rise to strong Raman band, we assign to this mode the relatively strong Raman line observed for $Rb_2MgWP$ at 399 $cm^{-1}$. The $\nu_4(WO_6)$ mode corresponds, most likely, to the 400–440 $cm^{-1}$ IR bands. The $\nu_6(WO_6)$ mode is difficult to assign since it is located in the same region as the lattice modes. We locate this mode close to 250 $cm^{-1}$.

In the lattice modes region, the translational modes of $K^+$, $Mg^{2+}$ and $PO_4^{3-}$ ions as well as librational modes of $PO_4^{3-}$ ions and $WO_6$ groups should be expected. The former studies of phosphates showed that it is difficult to distinguish between librational and translational modes of the $PO_4^{3-}$ ions, which were located in a broad wavenumber range, 100–300 $cm^{-1}$ [26]. The later studies of potassium–lanthanide phosphates and $Pb_3(PO_4)_2$ evidenced that the higher frequency modes have larger contribution of phosphate ions librations whereas the lower frequency modes have large contribution of translational motions of the phosphate ions [27,28]. Translational modes of heavy $Pb^{2+}$ ions were observed below 100 $cm^{-1}$ [28] but the frequency of these modes should increase significantly with atomic mass decrease and increase if covalent character of the metal–oxygen bonds is taken into account. As a result, the $T'$(Fe) and $T'$(Cr) modes in $Na_3Fe_2(PO_4)_3$ and $Na_3Cr_2(PO_4)_3$ phosphates were observed at 340–405 $cm^{-1}$ [26]. Since atomic mass of Mg is smaller than that of Fe or Cr but the Mg–O bond character less covalent, we may expect to observe $T'$(Mg) modes in a similar frequency range as $T'$(Fe) and $T'$(Cr) modes. We assign, therefore, the 330–380 $cm^{-1}$ bands to the $T'$(Mg) modes. The translations of $Rb^+$ ions should be observed at very low wavenumbers, since rubidium–oxygen distances are large and the corresponding interactions have strongly ionic character. The studies of KTP located $T'(K^+)$ modes at 96 and 120 $cm^{-1}$ [29], whereas the study of potassium–antimony phosphates located these modes below 150 $cm^{-1}$ [30]. On the other hand, in tungstates and perovskites the $T'(W^{6+})$ and $L(WO_6)$ modes appeared below 150 $cm^{-1}$ [31–33]. We assign, therefore, the weak bands below 140 $cm^{-1}$ to the coupled modes involving large contribution of the $Rb^+$ and $W^{6+}$ ions translations together with the librations of the $WO_6$ groups.

## 4. Conclusions

A replacement of $Rb^+$ for $K^+$ in $K_2MgWO_2(PO_4)_2$ appears to have a primary impact on the crystal structure and NLO properties. Unlike the other members of the $K_2M^{II}WO_2(PO_4)_2$ series, the present structure is centrosymmetric at room temperature and as such does not allow the second-harmonic generation. Besides, the structure of $Rb_2MgWO_2(PO_4)_2$ is not related to the structure of KTP, like $K_2MgWO_2(PO_4)_2$, but crystallizes in the new type of orthorhombic structure. The $MgO_6$ and $WO_6$ octahedra in this structure are not linked into infinite chains, like in the potassium analog, but are arranged into polyhedral groups consisting of two edge sharing $MgO_6$ joined by corners with two $WO_6$ octahedra. The common feature of KTP and this new structure is the presence of the tunnels occupied by alkali metal ions. Relatively high values of anisotropic thermal displacement amplitudes of $Rb^+$ indicate that these loosely bound ions perform thermally activated movements within the tunnels. This property allows for the fast ionic conductivity at elevated temperature.

Raman and IR spectra are consistent with the crystal structure. They show, for example, large splitting of the $\nu_3(PO_4)$ mode that indicates considerable distortion of the $PO_4^{3-}$ tetrahedra. The spectra show also that stretching

modes of $WO_6$ groups are observed at significantly higher frequency (839–913 $cm^{-1}$) than stretching modes of $TiO_6$ groups (600–850 $cm^{-1}$). The most intense Raman band is that one corresponding to the symmetric stretching mode of the $WO_6$ octahedron. Our results suggest that this mode can probably contribute to efficient stimulated Raman scattering, making $Rb_2MgWO_2(PO_4)_2$ a prospective material for the Raman laser application.

## References


[1] F.Z. Zumsteg, J.D. Bierlein, T.E. Gier, J. Appl. Phys. 47 (1976) 4980.
[2] J.D. Bierlein, H. Vanherzeele, J. Opt. Soc. Am. B 6 (1989) 622.
[3] I. Juwiler, A. Arie, A. Skliar, G. Rosenman, Opt. Lett. 24 (1999) 1236.
[4] J. Hellstrom, V. Pasiskevicius, F. Laurell, H. Karlsson, Opt. Lett. 24 (1999) 1233.
[5] J. Zhang, J. Wang, B. Ge, Y. Liu, X. Hu, R.I. Boughton, J. Cryst. Growth 267 (2004) 517.
[6] W.T.A. Harrison, T.E. Gier, G.D. Stucky, A.J. Schultz, Mater. Res. Bull. 30 (1995) 1341.
[7] P. Delarue, C. Lecomte, M. Jannin, G. Marnier, B. Menaert, Phys. Rev. B 58 (1998) 5287.
[8] G.D. Stucky, M.L.F. Phillips, T.E. Gier, Chem. Mater. 1 (1989) 492.
[9] P.A. Thomas, A.M. Glazer, B.E. Watts, Acta Crystallogr. B 46 (1990) 333.
[10] S.T. Norberg, J. Gustafsson, B.E. Mellander, Acta Crystallogr. B 59 (2003) 588.
[11] M. Simpson, W.T.A. Harrison, Solid State Sci. 6 (2004) 981.
[12] E.M. McCarron III, J.C. Calabrese, T.E. Gier, L.K. Cheng, C.M. Foris, J.D. Bierlein, J. Solid State Chem. 102 (1993) 354.
[13] U. Peuchert, L. Bohaty, Acta Crystallogr. C 51 (1995) 1719.
[14] U. Peuchert, L. Bohaty, J. Schreuer, Acta Crystallogr. C 53 (1997) 11.
[15] U. Peuchert, L. Bohaty, J. Schneider, J. Appl. Crystallogr. 31 (1998) 10.
[16] Oxford Diffraction, CrysAlis CCD Version 1.170.14, Oxford Diffraction Ltd., Oxford, UK, 2002.
[17] Oxford Diffraction, CrysAlis RED Version 1.170.14, Oxford Diffraction Ltd., Oxford, UK, 2002.
[18] G.M. Sheldrick, SHELXS97, Program for Solution of the Crystal Structures, University of Goettingen, 1997.
[19] G.M. Sheldrick, SHELXL99, Program for Crystal Structure Refinement, University of Goettingen, 1999.
[20] K. Nakamoto, Infrared and Raman Spectra of Inorganic and Coordination Compounds, Wiley, New York, 1986.
[21] G.E. Kugel, F. Brehat, B. Wyncke, M.D. Fontana, G. Marnier, C. Carabatos-edelec, J. Mangin, J. Phys. C 21 (1988) 5565.
[22] C.-S. Tu, A.R. Guo, R. Tao, R.S. Katiyar, J. Appl. Phys. 79 (1996) 3235.
[23] K. Vivekanandan, S. Selvasekarapandian, P. Kolandaivel, M.T. Sebastian, S. Suma, Mater. Chem. Phys. 49 (1997) 204.
[24] M.J. Bushiri, R.S. Jayasree, M. Fakhfakh, V.U. Nayar, Mater. Chem. Phys. 73 (2002) 179.
[25] M.J. Bushiri, V.U. Nayar, J. Nonlinear Opt. Phys. Mater. 10 (2001) 345.
[26] M. Barj, G. Lucazeau, C. Delmas, J. Solid State Chem. 100 (1992) 141.
[27] L. Benarafa, L. Rghioui, R. Nejjar, M. Saidi Idrissi, M. Knidiri, A. Loriaux, F. Wallart, Spectrochim. Acta 1 (61) (2005) 419.
[28] B. Mihailova, U. Bismayer, A. Engelhardt, B. Guttler, J. Phys. Condens. Matter. 13 (9) (2001) 9383.
[29] M.J. Bushiri, V.P. Mahadevan Pillai, R. Ratheesh, V.U. Nayar, J. Phys. Chem. Solids 60 (1999) 1983.
[30] E. Husson, F. Genet, A. Lachgar, Y. Piffard, J. Solid State Chem. 75 (1988) 305.
[31] M. Liegeois-Duyckaerts, P. Tarte, Spectrochim. Acta A 30 (1973) 1771.
[32] M. Maczka, J. Solid State Chem. 129 (1997) 287.
[33] M. Maczka, J. Hanuza, A.F. Fuentes, Y. Morioka, J. Phys.: Condens. Matter 16 (2004) 2297.